

# Grating-based microcavity with independent control of resonance energy and linewidth for non-Hermitian polariton system

Jiaqi Hu,<sup>1</sup> Nathaniel Lydick,<sup>2</sup> Zhaorong Wang,<sup>2</sup> F. Jabeen,<sup>3</sup> C. Schneider,<sup>3,4</sup> S. Höfling,<sup>3</sup> and Hui Deng<sup>1,2,\*</sup>

<sup>1</sup>*Applied Physics Program, University of Michigan, Ann Arbor, Michigan 48109, USA*

<sup>2</sup>*Department of Physics, University of Michigan, Ann Arbor, Michigan 48109, USA*

<sup>3</sup>*Technische Physik, Physikalisches Institut and  
Würzburg-Dresden Cluster of Excellence ct.qmat,  
Universität Würzburg, 97074 Würzburg, Germany*

<sup>4</sup>*Institute of Physics, University of Oldenburg, 26129 Oldenburg, Germany*

(Dated: August 25, 2022)

## Abstract

Exciton-polaritons have become an emerging platform for implementing non-Hermitian physics. The implementation commonly requires control of both the real and imaginary parts of the eigenmodes of the system. We present an experimental method to achieve this purpose using microcavities with sub-wavelength gratings as reflectors. The reflectivity and reflection phase of the grating can be changed by its geometric parameters and they determine the energy and linewidth of the polariton modes. We demonstrate that this method allows a wide range of possible polariton energy and linewidth, suitable for implementing non-Hermitian polariton systems with coupled modes.

Non-Hermitian physics [1] has been recently studied in many optical systems, which naturally involve gain and loss [2, 3]. Novel phenomena are expected near exceptional points, which are singularities of the spectrum in the parameter space spanned by the complex energies of different modes within the system and the coupling between the modes. Experimental observations range from uni-directional propagation [4, 5] to orbital angular momentum beam emission [6] and enhanced sensing [7].

A particularly interesting system for non-Hermitian physics is the exciton-polariton system, which allows the study of the interplay of non-Hermitian physics with nonlinearity-induced features such as superfluidity [8–10]. Exciton-polaritons are formed by strong-coupling between a photonic cavity mode and an exciton mode, each subject to gain and loss. Compared to typical optical systems, the exciton component introduces a much stronger nonlinearity. In a uniform polariton system, spontaneous condensation into different modes has been predicted depending on the phase space trajectory around the exceptional points [11], and adiabatic flipping between the photonic and excitonic modes was envisioned near the exception points [12]. These studies provide new insight to unique features of non-equilibrium phase transitions. Coupling multiple laterally localized polariton modes provides further freedom to engineer the non-Hermitian system and to access novel phenomena such as non-Hermitian skin effect due to effective non-reciprocal hopping [13–15] and synchronization among a large array via supersymmetry selection [16].

Exploring these phenomena often requires precise tuning of the system parameters, including the real and imaginary part of energies of the individual modes and the coupling strength between them. Such tuning is difficult with conventional cavities made of distributed Bragg reflectors (DBRs). While the cavity energy is readily tunable by a tapered cavity thickness, other parameters, such as the cavity decay rate, exciton energy and decay rate, and exciton-photon coupling, are generally not tunable in the same sample. Creating a polariton lattice, by etched micropillars or patterned metal layer deposited on top of the cavity [17], introduces a variable coupling among the localized polariton modes, yet it is challenging to decouple the energy and linewidth of the modes. Alternatively, spatially structured non-resonant optical pumps have also been used to introduce a potential landscape and provide polariton gain, leading to observations such as topological Berry phase [18], chiral state emission [19], condensation in topological defect state [20], and optical switching of condensates [21]. However, the pump introduces non-uniform and nonlinear modulations of multiple parameters of the system simultaneously. Understanding of the system properties often requires comparison between experiments and simulation for each device and pump configuration, making it difficult for *a priori* predictions as well as extensions to more complicated or large-scale lattices.

---

\* dengh@umich.edu

Here we demonstrate a method to independently control both the energy and linewidth of the photonic cavity mode, and consequently the polariton mode. It is based on a hybrid microcavity with a sub-wavelength grating and a DBR as the two reflectors [22]. The reflectivity and reflection phase of the grating, which affect the cavity decay rate and resonant energy respectively, can be tuned via the geometric parameters of the grating. The complex eigenenergy of the polariton is determined in a completely passive way during the fabrication of the device, which allows the device to be compatible with simple spatially uniform optical pumping or even electrical pumping. The gratings also define the in-plane spatial extent of the polariton mode, therefore allowing the creation of multiple localized modes with controllable coupling strengths that could be potentially extended to large scale devices, as demonstrated in Refs. [23, 24]. The polariton mode will be linearly polarized for the gratings we are using and the polarization is determined by the orientation of the grating. We demonstrate devices with a tuning range on the order of a few meV for the eigenenergy and from sub-meV to a few meV for the linewidth, appropriate for models that require the energy, linewidth, and coupling strength to be comparable [11, 12, 25].

High-contrast sub-wavelength gratings have been used as broad-band high reflectivity mirrors in cavities of both vertically emitting lasers and exciton polaritons [22, 26]. Particularly, for a square binary grating, whose cross-sectional profile is shown in Fig. 1(a), the mechanism of the high reflectivity can be understood as the cancelation of the zeroth-order Fourier component of two waveguide-array-like resonant modes of the grating structure at the output (transmission) interface [27]. The resonant frequency and field amplitude distribution of each of the modes are sensitive to the geometry of the grating bars with different dependencies. Therefore, a change in the period or duty cycle of the grating results in an overall change of the amplitude and phase of the reflected field. This allows us to tune the energy and linewidth of the cavity resonance locally.

To evaluate the accessible range of tuning, we first perform numerical simulations [28] with the Rigorous Coupled-Wave Analysis (RCWA) method [29] for a realistic grating mirror structure. The mirror consists of an  $\text{Al}_{0.2}\text{Ga}_{0.8}\text{As}$  grating on top of an  $\text{Al}_{0.85}\text{Ga}_{0.15}\text{As}$  layer, followed by a 1.5-pair DBR, with the DBR side facing an AlAs cavity. Fig. 1(b, c) shows an example of the zeroth-order reflectivity and reflection phase near a high-reflectivity region. The reflection is computed for 800 nm light with the electric field polarized perpendicularly to the grating bars and normal incidence from the AlAs side. For the one-dimensional gratings, the reflection properties can typically only be optimized for one of the orthogonal linear polarizations but not both simultaneously. In this example, for the polarization parallel to the grating bars the reflectivity in this parameter range is only about 0.5. The grating has a thickness of 242 nm and is optimized for high reflectivity at 800 nm. The period  $\Lambda$  and duty cycle  $\eta$  are the geometric tuning parameters and the highest reflectivity is obtained at  $(\Lambda_0, \eta_0) = (351 \text{ nm}, 0.54)$ . The thickness of the  $\text{Al}_{0.85}\text{Ga}_{0.15}\text{As}$  layer is chosen so that the reflection phase is  $\pi$  at the highest reflectivity.

As  $(\Lambda, \eta)$  are tuned away from  $(\Lambda_0, \eta_0)$  in the two-variable parameter space, the reflectivity decreases [Fig. 1(b)] while the reflection phase [Fig. 1(c)] changes monotonously in the vicinity. Therefore, by selecting certain combinations of period and duty cycle, it is possible to attain reflectivity and phase separately. The available ranges of the reflectivity and phase are not independent. With Fig. 1(b, c) as an example, given a fixed reflectivity, the corresponding  $(\Lambda, \eta)$  can only move on a contour line, corresponding to a limited range of phase. However, as we will show later, the ranges are often adequate.

In experiment, the thickness of the layers of the wafer as well as the parameters of the

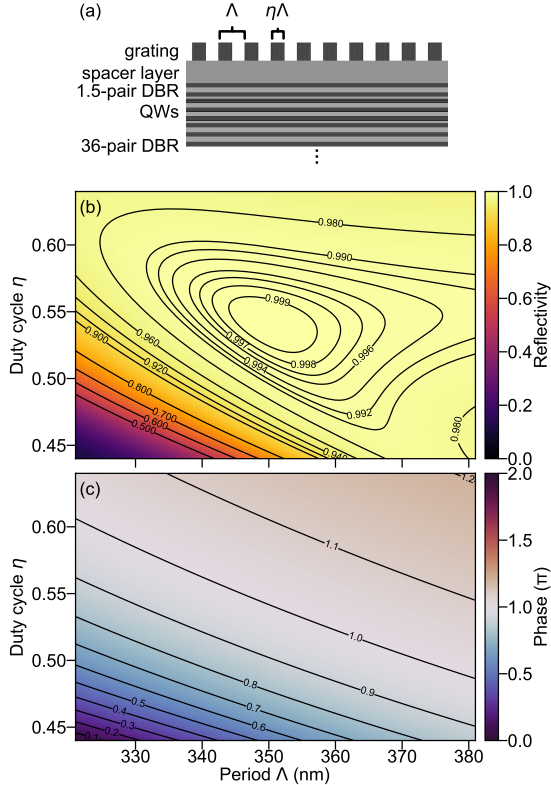


FIG. 1. (a) A schematic of the cross-sectional profile of the microcavity. Simulated zeroth-order reflectivity (b) and reflection phase (c) of a grating-based mirror as a function of the period and duty cycle of the grating, with 800 nm light polarized perpendicularly to the grating bars and normal incidence from the AlAs side.

grating may differ from the design, which can be calibrated through iterations between simulation and measurement of the energy and linewidth.

We fabricate the grating-based cavity devices on GaAs-based epitaxial wafers. These wafers have 12 GaAs/AlAs quantum wells, each of thickness 12 nm, distributed at three center anti-nodes of the resonant mode of an AlAs  $3\lambda/2$ -cavity. The lower mirror of the cavity is a  $\text{Al}_{0.15}\text{Ga}_{0.85}\text{As}/\text{AlAs}$  or  $\text{Al}_{0.2}\text{Ga}_{0.8}\text{As}/\text{AlAs}$  DBR with a total of 36 pairs of layers. The upper mirror is the aforementioned assembly of  $\text{Al}_{0.2}\text{Ga}_{0.8}\text{As}$  grating layer, an  $\text{Al}_{0.85}\text{Ga}_{0.15}\text{As}$  spacer layer, and 1.5 pairs of DBR. Each grating device is in a  $25\ \mu\text{m} \times 25\ \mu\text{m}$  or  $30\ \mu\text{m} \times 30\ \mu\text{m}$  square region, and many devices are made with different periods and duty cycles near the reflectivity maximum. The pattern is first written with e-beam lithography on a spin-coated ZEP520A e-beam resist layer of about 300 nm thickness, and then transferred to the grating layer with  $\text{BCl}_3$  reactive ion etching.

Fig. 2 shows photoluminescence (PL) spectra of typical devices in Fourier space, with a

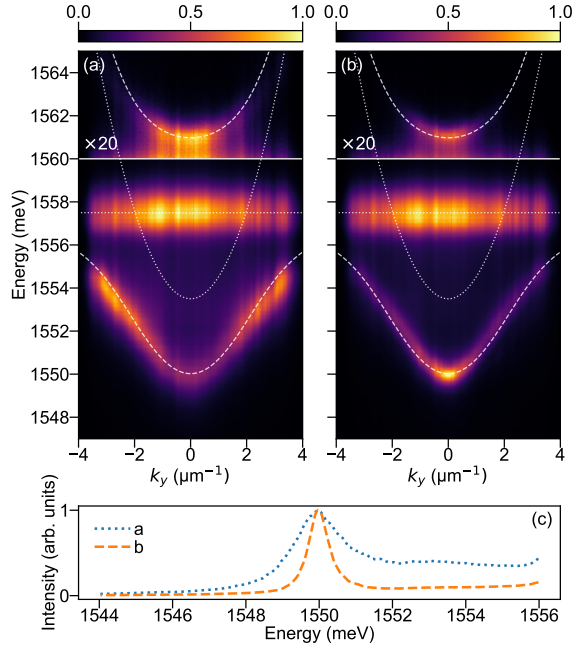


FIG. 2. Fourier space PL spectra of typical devices showing equal lower polariton energy but different linewidth. (a) Grating with designed period 324 nm and duty cycle 0.763. (b) Grating with designed period 348 nm and duty cycle 0.763. In subfigures (a) and (b), the horizontal axes are the wave vector parallel to the grating bars ( $k_y$ ). The spectra are collected with a polarizer perpendicular to the grating bars. The dashed lines are the polariton dispersions of a conventional DBR-DBR microcavity for comparison, calculated with a coupled oscillator model, assuming a quadratic cavity resonance dispersion. The parameters in the calculation are chosen to obtain the same exciton and polariton energies at zero wave vector as the measured devices, and the uncoupled exciton and cavity energies are marked with the dotted lines. (c) Line spectra near the lower polariton energy corresponding to (a) and (b), integrated within  $k_y < 0.1 \mu\text{m}^{-1}$  and normalized to the maximum value in the energy range.

polarizer perpendicular to the grating bars. The devices are pumped with a non-resonant continuous-wave laser focused to a  $2 \mu\text{m}$  spot in the center of the grating. Strong-coupling is evidenced by the emission from lower polariton and upper polariton branches for both devices in display. There is emission from near the exciton energy, due to the inhomogeneous broadening of the exciton [30] or emission from excitons with large wave vectors through first order diffraction of the grating. For the orthogonal polarization, the excitons remain in the weak-coupling regime.

These two devices provide an example of local linewidth control by the grating parameters. Their design parameters are  $\Lambda = 324 \text{ nm}$ ,  $\eta = 0.763$  [Fig. 2(a)] and  $\Lambda = 348 \text{ nm}$ ,  $\eta = 0.763$  [Fig. 2(b)]. The resulting lower polariton modes have nearly the same energy at

zero wave vector at  $(1549.98 \pm 0.02)$  meV and  $(1549.99 \pm 0.01)$  meV, but the linewidths are vastly different at  $(1.67 \pm 0.07)$  meV and  $(0.67 \pm 0.01)$  meV [Fig. 2(c)]. The Rabi splitting is  $\hbar\Omega_R \approx 10$  meV at zero wave vector, computed from the exciton energy measured in the unetched area near the device and both the upper and lower polariton energies. The dispersions of the cavity, and thus of the polaritons, have a small deviation from that of a conventional DBR-DBR microcavity with quadratic cavity resonance dispersion because the grating reflection phase also depends on the wave vector. The polariton dispersions of a conventional DBR-DBR microcavity are calculated with a coupled oscillator model and overlaid on the spectra for comparison, with parameters that result in the same exciton and polariton energies at zero wave vector as the measured devices and assuming a quadratic cavity resonance dispersion.

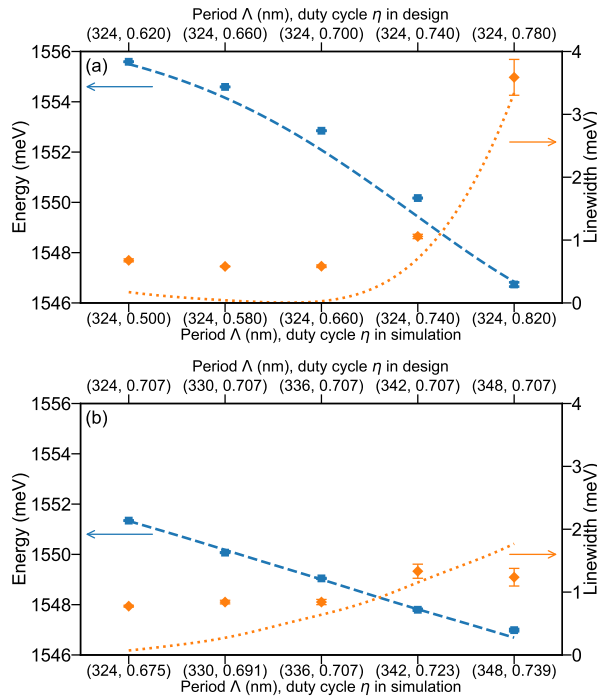


FIG. 3. Measured and simulated lower polariton energy and linewidth at zero wave vector, for two series of gratings shown in (a) and (b) respectively. (a) shows gratings designed to have the same period and varying duty cycles, while (b) shows varying period and same duty cycle. The upper horizontal axis labels the designed parameters while the lower horizontal axis labels the parameters used in simulation. The experimental energy (blue square markers) and linewidth (orange diamond markers) values are obtained by curve fitting of the PL spectra with Lorentzian peaks and the error bars represent the uncertainty of the corresponding fitting parameters calculated from the diagonal elements of the covariance matrix of the parameters. The simulated energy (dashed lines) and linewidth (dotted lines) values are obtained by curve fitting of the simulated reflection spectra with Fano lineshape.

To evaluate experimentally viable step sizes of the individual parameters, we fabricate

arrays of gratings with a range of different periods  $\Lambda$  and duty cycles  $\eta$ ; we then compare the design parameter values with values measured through scanning electron microscope (SEM), and compare the polariton energy and linewidth of these devices in RCWA simulated reflection spectra with measured values in PL [Fig. 3]. All RCWA simulations are performed with 41 basis functions and numerical convergence is verified.

The period  $\Lambda$  of the fabricated devices follows the design very well apart from a  $(2.8 \pm 0.4)\%$  offset above the designed values. This is consistent among devices with different parameters and is likely from an overall error in the calibration of the magnification of either the lithography or the measurement. The measured duty cycle  $\eta$  sometimes has a larger deviation from the design, due to the limitation of beam positioning accuracy of the e-beam lithography and due to insufficient anisotropy the etching process. For example, when the duty cycle is kept the same in the design and only the period is changed (near 340 nm), the duty cycle can still vary by 0.07 (about 24 nm). If the duty cycle is also varied in design, the discrepancy can be even larger, though the measurement uncertainty of the duty cycle is limited by the SEM to about 20 nm.

To calibrate the actual duty cycle more accurately, we compare the measured energy and linewidth of the devices with RCWA simulations where we fix the period at the designed value and allow duty cycle to be scaled linearly. As shown in Fig. 3, the measured linewidth follows qualitative the simulated results but are generally larger than the simulated linewidth. This is expected as the linewidth of the device is susceptible to imperfections in fabrication, such as sidewall roughness and surface scattering. The finite size of the gratings can also contribute to the broadening although it is not expected to be dominant here because the size of the devices is larger than 50 periods of grating [31, 32]. On the other hand, the polariton energies show excellent agreement between simulation and measurements.

From this result we estimate a step size of 6 nm for the period and 0.08 (26 nm) for the duty cycle. For our devices, these step sizes translate to polariton energy resolution of about 1 meV and linewidth resolution down to 0.5 meV. By mixing changes in both parameters, it is possible to obtain finer steps of polariton energy or linewidth. We also expect that the duty cycle step size can be further reduced to  $\lesssim 6$  nm with improvements to the fabrication process.

To evaluate how broadly we can separately tune the energy and linewidth, we fabricate arrays of gratings of varying  $\Lambda$  and  $\eta$  on  $5\text{ mm} \times 5\text{ mm}$  pieces of wafers. Fig. 4(a) and (b) show the measured PL energy and linewidth of lower polariton modes at zero wave vector from the gratings on two examples pieces respectively.

In general, the ranges of energy and linewidth are limited by the choice of the other value. To obtain a certain detuning, for example, will require the parameters to stay on a curve in the parameter space that gives the grating mirror the correct reflection phase for that cavity energy, and the reflectivity can only take values on that curve, limiting the linewidth. On the other hand, the reflectivity needs to be maintained at high enough values for strong-coupling and hence limits the range of detuning. For the piece shown in Fig. 4(a), the energy range spans more than 10 meV. For energies below 1550 meV, the linewidth range spans over 1.5 meV. For energies above 1550 meV, the linewidth is narrower and ranges between 0.24 meV and 0.92 meV. The reduced linewidth range is due to more positive detuning and smaller photonic fraction at these energies, as the linewidth variation comes from the photonic mode. Results from a similar wafer piece are shown in Fig. 4(b), where high-reflectivity is found in the parameter region near  $\Lambda \sim 550$  nm and  $\eta \sim 0.5$ . In this piece, for more than 5 meV of energy range, the linewidth can be tuned by more than

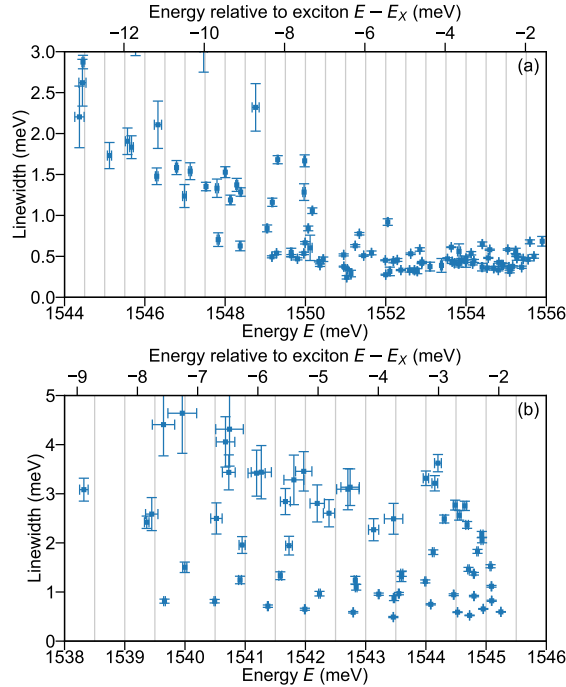


FIG. 4. A collection of measured PL energy and linewidth of lower polariton modes at zero wave vector of gratings with various parameters on two different sample pieces. (a) The gratings have designed periods around 336 nm and duty cycles around 0.72. (b) The gratings have designed periods around 550 nm and duty cycles around 0.50. Gray vertical lines mark 0.5 meV energy spacing. The experimental energy and linewidth values are obtained by curve fitting of the spectra with Lorentzian peaks and the error bars represent the uncertainty of the corresponding fitting parameters calculated from the diagonal elements of the covariance matrix of the parameters.

2 meV.

With these records as a calibration, a practical procedure can be followed to design and fabricate new devices that require local modes with different complex eigenenergies: first determine the target energy and linewidth, and then select the corresponding parameters that achieve those values from the present result.

Finally, with the tuning capabilities demonstrated, we consider the possibility of realizing a simple design of the non-Hermitian device that consists of two coupled local polariton modes. For such devices, it is often required that the coupling strength and the difference between the imaginary part of energies are comparable. It has been shown that sub-wavelength grating-based cavities can confine polariton modes in-plane to smaller than 10  $\mu\text{m}$ , and that these modes can be coupled to form dimer-like modes or one-dimensional chains [22, 23]. The coupling strength between neighboring modes is on the order of 0.5 meV [24], comparable to the tuning range of linewidth in the present case. In Fig. 4 vertical lines with 0.5 meV spacing are added in the background to show the available choices of linewidth within 0.5 meV energy bins.

In summary, we have demonstrated that grating-based microcavities can be used to create



polariton modes with controllable energy and linewidth. The polariton energy can be tuned over a range comparable to that of the normal mode splitting, while the linewidth can be independently tuned from a fraction of a meV to a few meV. The tuning resolution of 0.5–1 meV is mainly limited by the e-beam lithography resolution of 24 nm. Improvements in the fabrication accuracy, especially in the e-beam lithography, will enable finer tuning resolution. The demonstrated system is scalable to large lattices. The ability to accurately and independently tune the energy, loss and gain of the system may facilitate the study a wide range of non-Hermitian phenomena on the polariton platform [11, 12, 25, 33], and may also enable development of single photon or entangled photon sources based on coupled, driven polariton systems [34–36].

## ACKNOWLEDGMENTS

J.H., N.L., Z.W., and H.D. acknowledge financial support from the US National Science Foundation (NSF) under Grant No. DMR 2004287. C.S. acknowledges funding by the German Research Foundation (DFG) within the Project No. SCHN1376/13-1 and S.H. within the Project No. HO5194/12-1. This work was performed in part at the University of Michigan Lurie Nanofabrication Facility. We thank S. Brodbeck and P. Wyborski for their contributions to this work by epitaxial growth of samples. J.F., C.S., and S.H. gratefully acknowledge support of this work by the Free State of Bavaria.

## CONFLICT OF INTEREST

The authors have no conflicts to disclose.

## AUTHOR CONTRIBUTIONS

**Jiaqi Hu:** Conceptualization (equal); data curation (equal); formal analysis (equal); investigation (lead); methodology (equal); validation (equal); visualization (equal); writing – original draft (lead); writing – review and editing (equal). **Nathaniel Lydick:** Investigation (supporting); writing – review and editing (equal). **Zhaorong Wang:** Resources (equal). **F. Jabeen:** Resources (equal). **C. Schneider:** Resources (equal); writing – review and editing (equal). **S. Höfling:** Resources (equal); writing – review and editing (equal). **Hui Deng:** Conceptualization (equal); funding acquisition (equal); project administration (equal); supervision (equal); writing – original draft (supporting); writing – review and editing (equal).

## DATA AVAILABILITY STATEMENT

The data that support the findings of this study are available from the corresponding author upon reasonable request.

---

- [1] C. M. Bender, Making sense of non-Hermitian Hamiltonians, *Reports on Progress in Physics* **70**, 947 (2007).
- [2] S. Longhi, Parity-time symmetry meets photonics: A new twist in non-Hermitian optics, *EPL (Europhysics Letters)* **120**, 64001 (2017).
- [3] R. El-Ganainy, K. G. Makris, M. Khajavikhan, Z. H. Musslimani, S. Rotter, and D. N. Christodoulides, Non-Hermitian physics and PT symmetry, *Nature Physics* **14**, 11 (2018).
- [4] Z. Lin, H. Ramezani, T. Eichelkraut, T. Kottos, H. Cao, and D. N. Christodoulides, Unidirectional Invisibility Induced by  $\mathcal{PT}$ -Symmetric Periodic Structures, *Physical Review Letters* **106**, 213901 (2011).
- [5] L. Feng, Y.-L. Xu, W. S. Fegadolli, M.-H. Lu, J. E. B. Oliveira, V. R. Almeida, Y.-F. Chen, and A. Scherer, Experimental demonstration of a unidirectional reflectionless parity-time metamaterial at optical frequencies, *Nature Materials* **12**, 108 (2013).
- [6] P. Miao, Z. Zhang, J. Sun, W. Walasik, S. Longhi, N. M. Litchinitser, and L. Feng, Orbital angular momentum microlaser, *Science* **353**, 464 (2016).
- [7] W. Chen, Ş. Kaya Özdemir, G. Zhao, J. Wiersig, and L. Yang, Exceptional points enhance sensing in an optical microcavity, *Nature* **548**, 192 (2017).
- [8] H. Deng, H. Haug, and Y. Yamamoto, Exciton-polariton Bose-Einstein condensation, *Reviews of Modern Physics* **82**, 1489 (2010).
- [9] M. D. Fraser, Coherent exciton-polariton devices, *Semiconductor Science and Technology* **32**, 093003 (2017).
- [10] S. Ghosh and T. C. H. Liew, Quantum computing with exciton-polariton condensates, *npj Quantum Information* **6**, 1 (2020).
- [11] R. Hanai, A. Edelman, Y. Ohashi, and P. B. Littlewood, Non-Hermitian Phase Transition from a Polariton Bose-Einstein Condensate to a Photon Laser, *Physical Review Letters* **122**, 185301 (2019).
- [12] J. B. Khurgin, Exceptional points in polaritonic cavities and subthreshold Fabry–Perot lasers, *Optica* **7**, 1015 (2020).
- [13] S. Mandal, R. Banerjee, E. A. Ostrovskaya, and T. C. H. Liew, Nonreciprocal Transport of Exciton Polaritons in a Non-Hermitian Chain, *Physical Review Letters* **125**, 123902 (2020).
- [14] X. Xu, H. Xu, S. Mandal, R. Banerjee, S. Ghosh, and T. C. H. Liew, Interaction-induced double-sided skin effect in an exciton-polariton system, *Physical Review B* **103**, 235306 (2021).
- [15] H. Xu, K. Dini, X. Xu, R. Banerjee, S. Mandal, and T. C. H. Liew, Nonreciprocal exciton-polariton ring lattices, *Physical Review B* **104**, 195301 (2021).
- [16] M. P. Hokmabadi, N. S. Nye, R. El-Ganainy, D. N. Christodoulides, and M. Khajavikhan, Supersymmetric laser arrays, *Science* **363**, 623 (2019).
- [17] C. Schneider, K. Winkler, M. D. Fraser, M. Kamp, Y. Yamamoto, E. A. Ostrovskaya, and S. Höfling, Exciton-polariton trapping and potential landscape engineering, *Reports on Progress in Physics* **80**, 016503 (2017).

- [18] T. Gao, E. Estrecho, K. Y. Bliokh, T. C. H. Liew, M. D. Fraser, S. Brodbeck, M. Kamp, C. Schneider, S. Höfling, Y. Yamamoto, F. Nori, Y. S. Kivshar, A. G. Truscott, R. G. Dall, and E. A. Ostrovskaya, Observation of non-Hermitian degeneracies in a chaotic exciton-polariton billiard, *Nature* **526**, 554 (2015).
- [19] T. Gao, G. Li, E. Estrecho, T. C. H. Liew, D. Comber-Todd, A. Nalitov, M. Steger, K. West, L. Pfeiffer, D. W. Snoke, A. V. Kavokin, A. G. Truscott, and E. A. Ostrovskaya, Chiral Modes at Exceptional Points in Exciton-Polariton Quantum Fluids, *Physical Review Letters* **120**, 065301 (2018).
- [20] L. Pickup, H. Sigurdsson, J. Ruostekoski, and P. G. Lagoudakis, Synthetic band-structure engineering in polariton crystals with non-Hermitian topological phases, *Nature Communications* **11**, 4431 (2020).
- [21] Y. Li, X. Ma, Z. Hatzopoulos, P. Savvidis, S. Schumacher, and T. Gao, Switching off microcavity polariton condensate near the exceptional point, arXiv:2101.09478 [physics] (2021).
- [22] B. Zhang, Z. Wang, S. Brodbeck, C. Schneider, M. Kamp, S. Höfling, and H. Deng, Zero-dimensional polariton laser in a subwavelength grating-based vertical microcavity, *Light: Science & Applications* **3**, e135 (2014).
- [23] B. Zhang, S. Brodbeck, Z. Wang, M. Kamp, C. Schneider, S. Höfling, and H. Deng, Coupling polariton quantum boxes in sub-wavelength grating microcavities, *Applied Physics Letters* **106**, 051104 (2015).
- [24] S. Kim, Y. G. Rubo, T. C. H. Liew, S. Brodbeck, C. Schneider, S. Höfling, and H. Deng, Emergence of microfrequency comb via limit cycles in dissipatively coupled condensates, *Physical Review B* **101**, 085302 (2020).
- [25] P. Comaron, V. Shahnazaryan, W. Brzezicki, T. Hyart, and M. Matuszewski, Non-Hermitian topological end-mode lasing in polariton systems, *Physical Review Research* **2**, 022051 (2020).
- [26] P. Qiao, W. Yang, and C. J. Chang-Hasnain, Recent advances in high-contrast metastructures, metasurfaces, and photonic crystals, *Advances in Optics and Photonics* **10**, 180 (2018).
- [27] V. Karagodsky, F. G. Sedgwick, and C. J. Chang-Hasnain, Theoretical analysis of subwavelength high contrast grating reflectors, *Optics Express* **18**, 16973 (2010).
- [28] We use the numerical solver from Ref. [37].
- [29] M. G. Moharam and T. K. Gaylord, Rigorous coupled-wave analysis of planar-grating diffraction, *Journal of the Optical Society of America* **71**, 811 (1981).
- [30] R. Houdré, R. P. Stanley, and M. Ilegems, Vacuum-field Rabi splitting in the presence of inhomogeneous broadening: Resolution of a homogeneous linewidth in an inhomogeneously broadened system, *Physical Review A* **53**, 2711 (1996).
- [31] Y. Zhou, M. C. Y. Huang, and C. J. Chang-Hasnain, Large Fabrication Tolerance for VCSELs Using High-Contrast Grating, *IEEE Photonics Technology Letters* **20**, 434 (2008).
- [32] A. Tibaldi, P. Debernardi, and R. Orta, High-Contrast Gratings Performance Issues in Tunable VCSELs, *IEEE Journal of Quantum Electronics* **51**, 1 (2015).
- [33] K. Kawabata, K. Shiozaki, M. Ueda, and M. Sato, Symmetry and Topology in Non-Hermitian Physics, *Physical Review X* **9**, 041015 (2019).
- [34] T. C. H. Liew and V. Savona, Single Photons from Coupled Quantum Modes, *Physical Review Letters* **104**, 183601 (2010).
- [35] M. Bamba, A. Imamoglu, I. Carusotto, and C. Ciuti, Origin of strong photon antibunching in weakly nonlinear photonic molecules, *Physical Review A* **83**, 021802 (2011).
- [36] T. C. H. Liew and V. Savona, Multimode entanglement in coupled cavity arrays, *New Journal of Physics* **15**, 025015 (2013).

- [37] V. Liu and S. Fan, S4 : A free electromagnetic solver for layered periodic structures, *Computer Physics Communications* **183**, 2233 (2012).